Enhanced Tensile and Tear Toughness Properties of Thin-Wall Vacuum-Assisted High-Pressure Die-Cast Aural-5 Alloy by Friction Stir Processing

Avik Samanta, Hrishikesh Das, Glenn J. Grant, and Saumyadeep Jana

Abstract Steadily rising demand for glider weight reduction has driven the development of vacuum-assisted high-pressure die-cast (HPDC) Al alloys for automotive structural components. Aural-5 is a strontium-modified HPDC alloy utilizing manganese (Mn) to reduce die soldering, eliminating detrimental needle-shaped Fe-bearing β-phase intermetallic and improving ductility. HPDC Aural-5 contains shrinkage porosity, dendrites with Al-Si eutectic colonies, externally solidified crystals (ESCs), shear/band structure, and large second-phase particulates. Porosity, ESCs, and large second-phase particles work as crack initiation sites, negatively impacting tensile properties. In this study, friction stir processing (FSP) is employed for microstructural modification of a thin-walled HPDC Aural-5 by eliminating porosity and breaking down dendrites, second-phase particles, eutectic colonies, ESCs, and shear/band structures to create wrought microstructure with homogenized particle distribution. Mechanical property characterization indicates ~30 and ~35% enhancement in yield strength and ductility and associated marked effects on ~69% improvement in tear toughness according to the ASTM B871 test.

Keywords Friction stir processing · Aural-5 · Strength · Tear toughness · High pressure die-casting

Introduction

In recent decades, automotive original equipment manufacturers have been trying to produce a low-cost solution for vehicle lightweighting to meet zero carbon emission goals. To achieve that target, high-pressure die-cast (HPDC) aluminum castings alloys are increasingly used/considered for structural applications, e.g., shock towers, pillars, and floor rails for weight reduction. Multi-component, heavy structural steel load-bearing structural assemblies were replaced with single HPDC Al casting with intricate structural profiles to achieve similar functionality with less

A. Samanta · H. Das · G. J. Grant · S. Jana (✉)
Pacific Northwest National Laboratory, Richland, WA 99352, USA
e-mail: Saumyadeep.Jana@pnnl.gov

unpredictability [1]. The use of HPDC Al casting provides the opportunity for a reduction in part counts and weight. With the advancement of electric vehicles, hybrid powertrains and vehicle electrification are becoming ampler in the automotive industry. For lightweighting electric vehicles, HPDC Al castings can play a crucial role in designing lightweight housing for batteries and various powertrain and transmission components. Typical HPDC Al alloys use high Fe in alloy composition to avoid die soldering. However, high Fe content leads to the formation of needle-shaped β-AlFeSi$_5$ phases, which has harmful effects on the overall mechanical properties, especially ductility. Moreover, HPDC Al alloys contain gas and shrinkage porosity which act as a stress concentration and crack initiation sites under mechanical loading. HPDC Al alloys also contain acicular Si and large second-phase particulates, which negatively impact tensile strength and ductility [2, 3]. Therefore, the combination of a number of microstructural features and the alloy chemistry negatively impacts the mechanical properties [4] of HPDC Al alloys.

Improvements in die-casting technology (vacuum-assisted HPDC method and high vacuum die-casting method) help in reducing casting defects such as porosity [5]. Alloy chemistry is often altered to improve mechanical properties. Several low Fe containing premium HPDC Al alloy compositions (Silafont, Castasil, Aural, etc.) were developed with improved mechanical properties [6]. Adding 50–200 ppm of strontium (Sr) can transform acicular Si into a fine, fibrous structure [7, 8]. The ductility and manufacturability are significantly improved with the addition of Sr modifier without compromising strength. It satisfies the growing interests of the HPDC aluminum market. Although vacuum-assisted HPDC process with Sr- and more Mn-based material chemistry helped some of the issues of HPDC Al alloys, they still consist of shrinkage porosity in the middle section, dendritic microstructure with Al-Si eutectic colonies, shear/band structure beneath the die-wall, and large second-phase particulates.

This study applies friction stir processing (FSP) on thin-walled vacuum-assisted HPDC Aural-5 alloy, a popular Sr-modified premium quality Al alloy primarily used for automobile structural components. FSP is a widely used thermomechanical processing tool to effectively eliminate casting defects and modify the cast microstructure of aluminum alloys [9, 10]. FSP imposes severe plastic deformation on the workpiece material through a rotating tool-driven complex material mixing and microstructural change. As a result, the mechanical and metallurgical properties of workpiece material are altered through dynamic recrystallization and refinement of constituent phases [11]. FSP can elevate the tensile properties of HPDC Al alloys through porosity elimination and microstructure refinement [12]. FSP-driven microstructure modification can lead to enhanced strength and ductility [13] and associated marked effects on improved resistance to fatigue failure [14] and fracture toughness [15]. This study investigates FSP-driven microstructural modification on Aural-5 and change in tensile properties. Finally, tear toughness and strength are compared between FSP and without FSP according to the ASTM B871 test.

Experimental Methods

This study conducted FSP trials on HPDC Aural-5, a Sr-modified and low Fe (~0.09 wt.%) containing alloy. FSP experiments were carried out on flat plate geometry. The thickness of Aural-5 plates was measured to be 2.4 ± 0.1 mm. The nominal composition of Aural-5 is reported in Table 1.

For FSP experiments, a scrolled shoulder tool was used, as shown in Fig. 1a. The tool has a conical threaded pin with three flat segments equally separating the threads. Position control mode is used during FSP experiments. Penetration depth was kept at 2.15 mm. Tool rotation is counterclockwise at 2° tilt angle for single-pass FSP experiments. Therefore, the advancing side (AS) and retreating side (AS) are illustrated in Fig. 1b. After several initial experiments, one FSP condition was chosen, which gives defect-free microstructure consolidation. The tool rotational speed was kept at 1200 RPM, and the traverse speed was 0.7 m/min.

Metallographic specimens were extracted from the as-cast and nugget zone of FSPed samples for microstructure characterization. In addition, full-thickness subsize ASTM E8 specimens were machined from the middle of the nugget region, as shown in Fig. 1b, and from an unprocessed Aural-5 plate to characterize the tensile properties. Gauge length and width of bulk tensile specimens were kept at 15.8 and 3.4 mm. During the tensile testing, a computer-controlled tester set the initial crosshead velocity as 0.005 mm s^{-1} at room temperature.

Table 1 Elemental composition of Aural-5

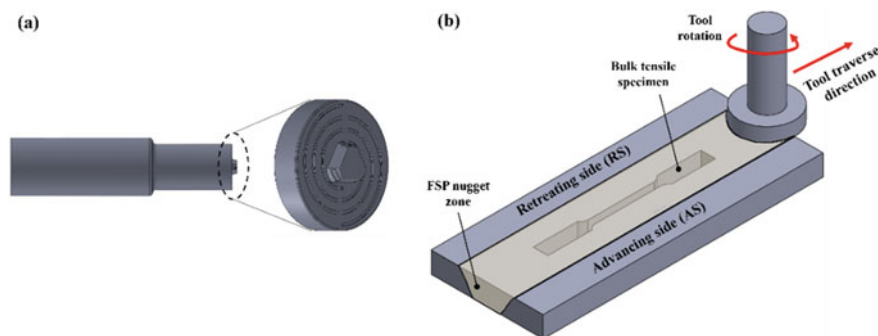| Al	Si	Mg	Mn	Fe	Ti	Sr
Balance	6.88	0.25	0.56	0.09	0.06	125 ppm

Fig. 1 **a** Schematic representation of the FSP tool used in the study, **b** location of tensile specimen with respect to FSP nugget

Results and Discussion

Microstructure Evolution

The microstructure of as-cast HPDC Aural-5 is characterized before performing any FSP experiments. A typical low-magnification full-thickness cross-sectional image of HPDC Aural-5 is shown in Fig. 2a. Most of the porosity is concentrated near the middle section, whereas the die-wall areas are mostly porosity-free. As illustrated in Fig. 2b, which is a higher magnification view of the red rectangle of Fig. 2a, shows three distinct layers of microstructure: (1) a surface layer or die-wall, (2) a middle layer or mid-wall, and (3) a layer between the surface layer and middle layer (the so-called shear/defect band). The surface layer is ~200–250 μm thick with a very refined microstructure and little to no porosity. The middle layer contains high porosity. Most porosity is shrinkage porosity, as illustrated in Fig. 2c. The die-casting industry typically observes these two layers [16]. Less porous, refined microstructure at die-wall is generated through faster solidification during the HPDC process, and a relatively slower solidification rate determines coarse porous microstructure of mid-wall. A third layer of microstructure named as shear/defect band is observed for Aural-5 in between die-wall and mid-wall. A shear band is typically formed in some HPDC and vacuum-assisted HPDC Al and Mg alloy containing very fine and dendritic primary grains with high percentage of eutectic colonies [17]. It is formed by slip between the surface layer and the inner adjacent region due to significant shear occurring either during die filling or during pressure intensification [18].

A typical higher magnification micrograph of HPDC Aural-5 is shown in Fig. 3a, indicating that it contained large dendritic externally solidified crystals (ESCs) and disintegrated ESCs in between the in-cavity solidified primary grains and eutectic (marked by blue arrows). The ESCs are nucleated and grown externally within the shot chamber before being injected into the HPDC cavity. ESCs can have an adverse effect on tensile properties by expediting the crack initiation and propagation under loading [19]. As shown in Fig. 3a, the ESCs and fragmented ESCs were much larger than the in-cavity solidified grains [17]. Most ESCs and fragmented ESCs were located in the mid-wall; however, there was a small fraction of ESCs in the die-wall and shear band. Additionally, Fe–Mn-containing second-phase particles can be seen
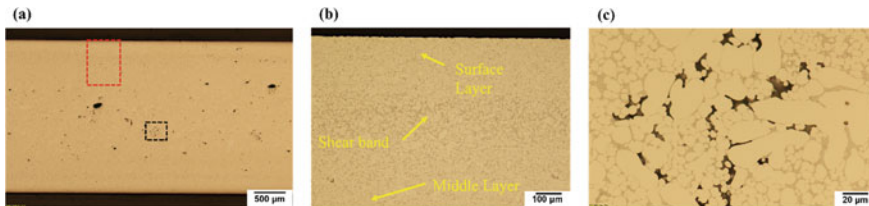

Fig. 2 Microstructure of vacuum-assisted HPDC Aural-5 plate: **a** overview of the cross-section; **b** shear/defect band formation below die-wall/skin; and **c** shrinkage porosity in the middle section
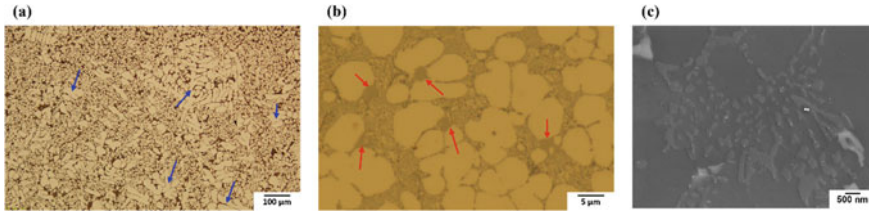
Fig. 3 Presence of **a** a mixture of large dendritic ESCs and fragmented ESCs; **b** large second-phase particles; and **c** fine fibrous eutectic Si structure

between the dendrites (marked by red arrows in Fig. 3b). The addition of Sr led to an extensive refinement of the morphology of eutectic Si. As illustrated in Fig. 3c, Al–Si eutectic colonies contain fine fibrous networks of eutectic Si.

To study cross-sectional micrographs of FSPed plate, metallography specimens were extracted at 125 mm away from the plunge location. Figure 4a illustrates a microstructural overview at low-magnification of Aural-5 after FSP. The basin-shaped nugget region has distinct AS and more diluted RS boundaries. Two locations within the nugget zone of the FSP2 were chosen for a detailed study of the microstructure. In Fig. 4b, a high magnification image of the FSP-HPDC interface shows the transition of the FSPed microstructure to the parent HPDC microstructure. A gradual change is observed from the dendritic structure in the as-cast region to the wrought microstructure in the processed zone. Within the nugget zone, as-cast dendrites are disintegrated to form a wrought microstructure. A thermomechanical affected zone (TMAZ) works as a transition zone from the severe plastic deformation zone to the as-cast material. In Fig. 4c, a high magnification image of the nugget zone shows that dendrites and Al-Si eutectic colonies were fragmented. This location was at the same position as the surface-layer edge. Therefore, it can be concluded that the FSP processing eliminated the high-density eutectic regions and made a more uniform distribution of elements across the cross section. In addition, the ESCs were also eliminated after FSP. Furthermore, the shrinkage porosities were removed completely from the middle section after FSP, and second-phase particles were refined.

Tensile Properties

Eight full thickness E8 specimens for HPDC condition and three for FSP condition were tested. Figure 5 compares the engineering stress versus percent elongation plot between two specimens from HPDC and FSPed conditions. Those two specimens denoted the maximum and minimum ductility of each condition, and others fell in between. It shows that FSP can increase yield strength and % elongation to failure after processing. The yield strength (YS) of HPDC Aural-5 alloy is ~101.3 ± 5.5 MPa, whereas that is increased by ~30% to ~131.5 ± 3.8 MPa after FSP. The change in
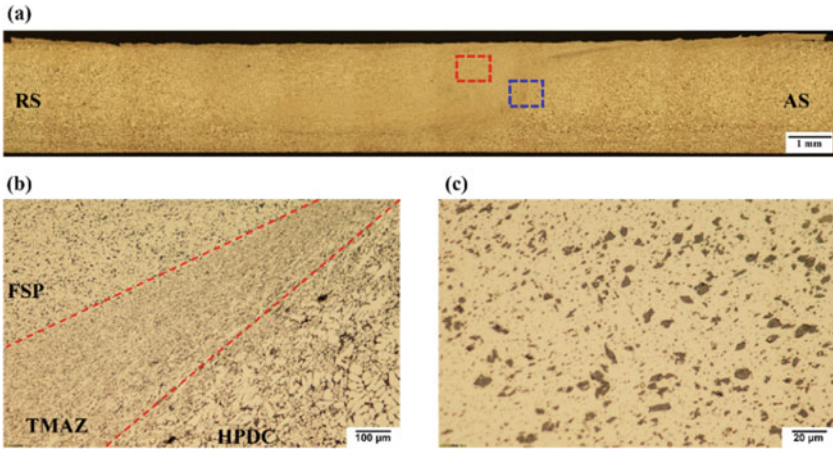
Fig. 4 Cross-sectional microstructural features of FSPed Aural-5 alloy plate: **a** nugget zone shape and size; **b** interface between HPDC and FSP regions; **c** wrought microstructure with uniformly distributed Si and second-phase particles

UTS is statistically insignificant. It is ~243.8 ± 6.6 MPa after FSP compared to 257.4 ± 11.7 MPa for the as-cast Aural-5 condition. Aural-5 was a highly ductile material; however, FSP was still able to improve the ductility further. The elongation to failure for HPDC Aural-5 was 13.5 ± 3.8%, whereas after FSP, it increased by 35% to 18.3 ± 1.7%.

Fig. 5 Comparison of engineering stress versus percent elongation between HPDC and FSP condition
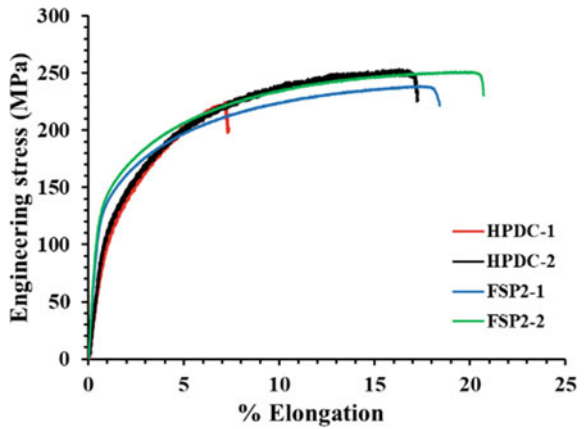
Tear Toughness

According to ASTM standard B871-01 [20], standard tear test specimens were machined for HPDC and FSPed material. The schematic of specimen geometry is illustrated in Fig. 6a. The rectangular-shaped tear test specimens have an 11 mm deep 60° V-notch with a 0.025 mm notch radius. For FSP, the specimens were machined in two different orientations. In transverse orientation, the notch tip was placed 2 mm inside the boundary of the AS. The notch tip was placed along the centerline of the tool traverse direction for longitudinal orientation. After placing the specimen in MTS 810 materials testing system with a 10 kN load cell, 220 N preload was applied. During the test, a loading rate of 0.02 mm/s was used at ambient temperature and force–displacement data were recorded. In addition, thickness and net section width between the notch root and back edge of the specimen was measured, and the load–displacement data were normalized accordingly.

The tear test is very useful as an indicator of the toughness of thin aluminum sheets. Representative force–displacement curves of HPDC and two orientations of FSPed Aural-5 are illustrated in Fig. 6b. The slopes of the loading part of the curves are very similar to each other. However, both FSP configurations required higher force to initiate crack than HPDC. Additionally, FSP in longitudinal configuration needed more force than FSP in transverse configuration. Total energy required for crack initiation and propagation is calculated by numerical integration of the area under the force–displacement curve. As illustrated in Fig. 6c, FSPed specimens required higher energies for crack initiation and propagation than HPDC specimens. Therefore, FSP treatment on Aural-5 induced higher tear toughness and resistance to crack initiation and propagation than the HPDC condition in longitudinal and transverse orientation.
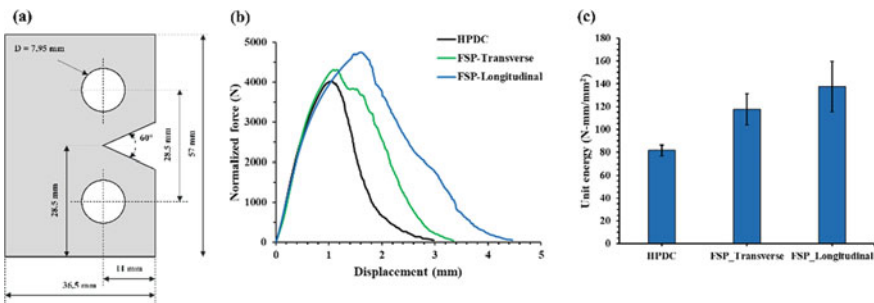

Fig. 6 Tear toughness test: **a** sample geometry; and comparison of **b** the force–displacement curve and **c** unit total energy

Conclusion

The microstructure of vacuum-assisted HPDC Aural-5 alloy consists of process-related high shrinkage porosity in the mid-wall area, α-Al dendrites, presence of ESCs, surface-layer edge beneath the die-wall with a high volume fraction of Al–Si eutectic colonies and large second-phase particles. Even though Sr modification significantly refined eutectic silicon and vacuum assistance reduced porosity in Aural-5, there is significant variation in the strength and ductility. After FSP, the as-cast microstructure is substantially modified by eliminating porosity, breaking down α-Al dendrites into a wrought microstructure. It also eliminates ESCs and breaks down Al–Si eutectic colonies into uniform distribution of fragmented Si particles. The shear/band structure is also broken down during FSP. The Fe–Mn-containing second-phase particles are also refined to some extent and redistributed homogeneously across the processed zone. This microstructure modification significantly improved tensile strength and ductility. Additionally, FSP-modified microstructure demonstrates more resistance to tear and an increase in tear toughness.

References

1. COSMO International (2014) Aluminum high pressure die casting
2. Hartlieb M (2013) Aluminum alloys for structural die casting. In: Die casting engineer, pp 40–43
3. Outmani I, Fouilland-Paille L, Isselin J, el Mansori M (2017) Effect of Si, Cu and processing parameters on Al-Si-Cu HPDC castings. J Mater Process Technol 249:559–569. https://doi.org/10.1016/j.jmatprotec.2017.06.043
4. Sigworth GK, Donahue RJ (2021) The metallurgy of aluminum alloys for structural high-pressure die castings. Int J Metalcast 15:1031–1046. https://doi.org/10.1007/s40962-020-00535-x
5. Niu XP, Hu BH, Pinwill I, Li H (2000) Vacuum assisted high pressure die casting of aluminium alloys. J Mater Process Technol 105:119–127. https://doi.org/10.1016/S0924-0136(00)00545-8
6. Rowe J (2012) Advanced materials in automotive engineering. Woodhead Publishing
7. Sigworth GK (2008) The modification of Al-Si casting alloys: important practical and theoretical aspects. Int J Metalcast 2:19–40. https://doi.org/10.1007/BF03355425
8. Hegde S, Prabhu KN (2008) Modification of eutectic silicon in Al-Si alloys. J Mater Sci 43:3009–3027. https://doi.org/10.1007/s10853-008-2505-5
9. Sharma SR, Ma ZY, Mishra RS (2004) Effect of friction stir processing on fatigue behavior of A356 alloy. Scr Mater 51:237–241. https://doi.org/10.1016/j.scriptamat.2004.04.014
10. Tsai FY, Kao PW (2012) Improvement of mechanical properties of a cast Al-Si base alloy by friction stir processing. Mater Lett 80:40–42. https://doi.org/10.1016/j.matlet.2012.04.073
11. Sun N, Apelian D (2011) Friction stir processing of aluminum cast alloys for high performance applications. JOM 63:44–50. https://doi.org/10.1007/s11837-011-0190-3
12. Samanta A, Seffens RJ, Das H et al (2022) Microstructure-refinement–driven enhanced tensile properties of high-pressure die-cast A380 alloy through friction stir processing. J Manuf Process 78:352–362. https://doi.org/10.1016/j.jmapro.2022.04.027
13. Rao AG, Deshmukh VP, Prabhu N, Kashyap BP (2015) Ductilizing of a brittle as-cast hypereutectic Al-Si alloy by friction stir processing. Mater Lett 159:417–419. https://doi.org/10.1016/j.matlet.2015.07.006

14. Jana S, Mishra RS, Baumann JB, Grant G (2010) Effect of friction stir processing on fatigue behavior of an investment cast Al-7Si-0.6 Mg alloy. Acta Mater 58:989–1003. https://doi.org/10.1016/j.actamat.2009.10.015

15. Abubaker HM, Merah N, Al-Badour F et al (2021) Influence of friction stir processing on wear, corrosion, and fracture toughness behavior of 2507 super duplex stainless steel. J Mater Eng Perform 30:89–102. https://doi.org/10.1007/s11665-020-05325-4

16. Yang KV, Cáceres CH, Nagasekhar AV, Easton MA (2012) The skin effect and the yielding behavior of cold chamber high pressure die cast Mg-Al alloys. Mater Sci Eng A 542:49–55. https://doi.org/10.1016/j.msea.2012.02.029

17. Gourlay CM, Laukli HI, Dahle AK (2007) Defect band characteristics in Mg-Al and Al-Si high-pressure die castings. Metall Mater Trans A 38:1833–1844. https://doi.org/10.1007/s11661-007-9243-1

18. Otarawanna S, Laukli HI, Gourlay CM, Dahle AK (2010) Feeding mechanisms in high-pressure die castings. Metall Mater Trans A 41:1836–1846. https://doi.org/10.1007/s11661-010-0222-6

19. Jiao XY, Zhang YF, Wang J et al (2021) Characterization of externally solidified crystals in a high-pressure die-cast AlSi10MnMg alloy and their effect on porosities and mechanical properties. J Mater Process Technol 298. https://doi.org/10.1016/j.jmatprotec.2021.117299

20. ASTM standard, Designation: B871-01, Standard Test Method for Tear Testing of Aluminum Alloy Products (Current edition approved April 1, 2007. Published May 2007. Originally approved in 1996. Last previous edition approved in 2001 as B 871–01) (2007)